Published in final edited form as:
Neuroscience. 2008 December 10; 157(4): 850–863. doi:10.1016/j.neuroscience.2008.09.043.

Dopaminergic innervation of interneurons in the rat basolateral amygdala

Courtney R. Pinard, **Jay F. Muller**, **Franco Mascagni**, and **Alexander J. McDonald***
Department of Pharmacology, Physiology and Neuroscience University of South Carolina School of Medicine, Columbia, SC 29208

Abstract

The basolateral nuclear complex of the amygdala (BLC) receives a dense dopaminergic innervation that plays a critical role in the formation of emotional memory. Dopamine has been shown to influence the activity of BLC GABAergic interneurons, which differentially control the activity of pyramidal cells. However, little is known about how dopaminergic inputs interface with different interneuronal subpopulations in this region. To address this question, dual-labeling immunohistochemical techniques were used at the light and electron microscopic levels to examine inputs from tyrosine hydroxylase-immunoreactive (TH+) dopaminergic terminals to two different interneuronal populations in the rat basolateral nucleus labeled using antibodies to parvalbumin (PV) or calretinin (CR). The basolateral nucleus exhibited a dense innervation by TH+ axons. Partial serial section reconstruction of TH+ terminals found that at least 43–50% of these terminals formed synaptic junctions in the basolateral nucleus. All of the synapses examined were symmetrical. In both TH/PV and TH/CR preparations the main targets of TH+ terminals were spines and distal dendrites of unlabeled cells. In sections dual-labeled for TH/PV 59% of the contacts of TH+ terminals with PV+ neurons were synapses, whereas in sections dual-labeled for TH/CR only 13% of the contacts of TH+ terminals with CR+ cells were synapses. In separate preparations examined in complete serial sections for TH+ basket-like innervation of PV+ perikarya, most (76.2%) of TH+ terminal contacts with PV+ perikarya were synapses. These findings suggest that PV+ interneurons, but not CR+ interneurons, are prominent synaptic targets of dopaminergic terminals in the BLC.

Keywords

electron microscopy; immunocytochemistry; parvalbumin; calretinin

The basolateral nuclear complex of the amygdala (BLC), consisting of the basolateral, lateral, and basomedial amygdalar nuclei, receives a dense dopaminergic innervation from the ventral tegmental area and substantia nigra (Fallon and Ciofi, 1992; Asan, 1993, 1997, 1998). These projections play a major role in the generation of both aversive and appetitive behaviors by the amygdala. Release of DA during stress is much higher in the BLC than in other targets of the mesolimbic DA system (Coco et al., 1992; Inglis and Moghaddam, 1999), and dopaminergic projections to the BLC are critical for fear conditioning and other aversive behaviors (Pezze and Feldon, 2004; LaLumiere et al., 2004). Dopaminergic inputs to the amygdala also play a

*Correspondence to: Alexander Joseph McDonald, Telephone: 803-733-3378 Fax: 803-733-1523, E-mail: mcdonald@med.sc.edu.
Section Editor: Charles Gerfen (Neuroanatomy)

role in the behavioral response to rewarding stimuli (Nakano et al., 1987), the reinforcing actions of cocaine (Wilson et al., 1994; Caine et al., 1995), and drug-stimulus learning that triggers relapse to drug-seeking behavior (See, 2005). In addition, dopaminergic afferents to the amygdala are implicated in schizophrenia, which is associated with an increase in amygdalar dopamine (Reynolds 1983).

Dopaminergic terminals form synapses with neurons in the BLC of the rat amygdala (Asan 1997). Although most of the structures innervated were distal dendrites and spines of unlabeled neurons, appositions were found on a few interneurons in the BLC (Asan 1997). Because different subpopulations of BLC neurons exhibit specific connections (Muller et al., 2003, 2005, 2006, 2007), understanding the effects of dopaminergic neurotransmission on information processing by the BLC will require knowledge of the innervation of distinct cell types by dopaminergic axon terminals. Previous studies have shown that there are two major cell classes in the BLC, pyramidal neurons and nonpyramidal neurons. Although these cells do not exhibit a laminar or columnar organization, their morphology, synaptology, electrophysiology, and pharmacology are remarkably similar to their counterparts in the cerebral cortex (Carlsen and Heimer, 1988; McDonald, 1992a; Washburn and Moises, 1992; Rainnie et al., 1993; Paré et al., 2003; Muller et al., 2005, 2006, 2007). Thus, pyramidal neurons in the BLC are projection neurons with spiny dendrites that utilize glutamate as an excitatory neurotransmitter, whereas most nonpyramidal neurons are spine-sparse interneurons that utilize γ-aminobutyric acid (GABA) as an inhibitory neurotransmitter. Recent dual-labeling immunohistochemical studies suggest that the BLC contains at least four distinct subpopulations of GABAergic interneurons that can be distinguished on the basis of their content of calcium-binding proteins and peptides. These subpopulations are: 1) parvalbumin +/calbindin+ neurons; 2) somatostatin+/calbindin+ neurons, 3) small bipolar and bitufted interneurons that exhibit extensive colocalization of vasoactive intestinal peptide, calretinin, and cholecystokinin; and 4) large multipolar cholecystokinin+ neurons that are often calbindin + (Kemppainen and Pitkänen, 2000; McDonald and Betette, 2001; McDonald and Mascagni, 2001, 2002; Mascagni and McDonald, 2003).

Dopamine has been shown to influence the activity of BLC GABAergic interneurons, which differentially control the activity of pyramidal cells (Rosenkranz and Grace, 1999; Bissiere et al., 2003; Loretan et al., 2004; Kroner et al., 2005). Parvalbumin-positive (PV+) and calretinin-positive (CR+) neurons are the predominant interneuronal subpopulations in the BLC (McDonald and Mascagni, 2001; Mascagni and McDonald, 2003). CR+ interneurons make up about 25–30% of BLC GABAergic interneurons and heavily innervate other interneurons, as well as pyramidal cells (McDonald and Mascagni, 2001; Muller et al., 2003). PV+ interneurons make up about 40% of GABAergic interneurons in the BLC, and are the main source of the perisomatic innervation of pyramidal cells (Muller et al., 2006). As in the cortex (Lewis et al., 1999; Yang et al. 1999; Benes & Berretta 2001), the action of dopamine on BLC neuronal activity and subsequent affective responses may depend, in part, on the specific populations of interneurons innervated.

Dual-labeling immunohistochemical studies at the light microscopic level have revealed that dopaminergic pericellular baskets envelope a subpopulation of PV-immunoreactive interneurons (Brinley-Reed and McDonald, 1999), many of which are known to be fast-spiking (Rainnie et al., 2006; Woodruff and Sah 2007b). In vitro electrophysiological studies in the lateral nucleus of the BLC have shown that dopamine enables the induction of LTP by increasing disynaptic inhibition of fast-spiking interneurons involved in feedforward inhibition (Bissiere et al., 2003). In addition, dopamine increases evoked and spontaneous spike firing of fast-spiking interneurons (Rosenkranz and Grace 1999; Kroner et al., 2005) and increases network activity (Loretan et al., 2004). A detailed knowledge of the DA innervation of BLC interneurons would be helpful in elucidating the mechanisms of dopaminergic modulation. The

present investigation is the first study to use dual-labeling electron microscopy to determine whether dopaminergic terminals synapse with distinct subclasses of local circuit neurons that contain the calcium-binding proteins parvalbumin (PV) or calretinin (CR) in the BLC.

EXPERIMENTAL PROCEDURES

Tissue preparation

All experiments were performed in male Sprague-Dawley rats (250–350 g; Harlan), were carried out in accordance with the National Institutes of Health Guide for the care and use of laboratory animals, and were approved by the University of South Carolina Institutional Animal Care and Use Committee. For light and confocal microscopy, rats were anesthetized with chloral hydrate (350 mg/kg), and perfused intracardially with phosphate buffered saline (PBS; pH 7.4) containing 1% sodium nitrite (50 ml) followed by 4% paraformaldehyde in phosphate buffer (PB; pH 7.4) (500 ml). Brains were removed and postfixed in the perfusate for 3 hours. For electron microscopy, and in one light microscopic preparation, rats were anesthetized and perfused intracardially with PBS containing 1% sodium nitrite (50 ml), followed by an acrolein/paraformaldehyde mixture (2.0% paraformaldehyde-3.75% acrolein in PB for 1 minute, followed by 2.0% paraformaldehyde in PB for 30 minutes). Following removal, acrolein-fixed brains were postfixed in 2.0% paraformaldehyde for 2 hours. Brains were sectioned on a vibratome in the coronal plane at either 50 μm (for light microscopy) or 60 μm (for electron microscopy). Sections through the anterior basolateral nucleus (BLa) (bregma levels −2.1 through −3.0: Paxinos and Watson, 1986) and posterior basolateral nucleus (BLp) (bregma levels −3.1 through −3.8: Paxinos and Watson, 1986) were processed for immunocytochemistry in the wells of tissue culture plates.

Light microscopic peroxidase immunohistochemistry

Single-label localization of tyrosine hydroxylase (TH) was performed in 3 rats using a mouse monoclonal antibody to TH (1:1000; clone LNC1, catalog #MAB318, Chemicon International Inc., Temecula, CA). Antibodies were diluted in PBS containing 0.4% Triton X-100 and 1% normal goat serum. Sections were incubated in primary antibody overnight at 4° C and then processed for the avidin-biotin immunoperoxidase technique using a biotinylated goat anti-mouse secondary antibody (1:500; Jackson ImmunoResearch Laboratories, Inc., West Grove, PA) and a Vectastain standard ABC kit (Vector Laboratories, Burlingame, CA). Nickel-enhanced DAB (3, 3′-diaminobenzidine-4HCl, Sigma Chemical Co., St. Louis, MO) was used as a chromogen to generate a black reaction product (Hancock, 1986). Following the immunohistochemical procedures, sections were mounted on gelatinized slides, dried overnight, dehydrated in ethanol, cleared in xylene, and coverslipped in Permount (Fisher Scientific, Pittsburgh, PA). In two of the four rats some sections were Nissl-counterstained with 1% Pyronin Y to label neuronal perikarya in the amygdala. Sections were analyzed using Olympus BHA and Nikon Eclipse E600 microscopes. Digital light micrographs were taken with a QImaging MicroPublisher 5.0 CCD camera (QImaging Corp., Burnaby, British Columbia). Brightness and contrast were adjusted using Photoshop 6.0 software.

Confocal microscopic fluorescence immunohistochemistry

Dual localization studies were performed in 3 rats using the mouse monoclonal TH antibody (1:1000; see above), a rabbit polyclonal TH antibody (1:1000; catalog #CA-101 bTHrab, Protos Biotech Corp., New York, NY), and a mouse monoclonal antibody to dopamine-beta-hydroxylase (DBH; 1:1000; clone 4F10.2, catalog #MAB308, Chemicon International Inc., Temecula, CA), the synthetic enzyme for norepinephrine, to determine the extent to which the monoclonal TH antibody stains norepinephrine-containing axons in the BLC. Sections were incubated overnight at 4° C in a cocktail of the rabbit polyclonal TH antibody combined with either the mouse monoclonal TH antibody or the mouse monoclonal DBH antibody. After

incubation in the primary antibody cocktail, sections were rinsed in 3 changes of PBS (10 min each) and then incubated in a cocktail of goat anti-rabbit Alexa-568 and goat anti-mouse Alexa-488 labeled secondary antibodies (1:400; Molecular Probes, Eugene, OR) for 3 hrs at room temperature. All secondary antibodies were highly cross-adsorbed by the manufacturer to ensure specificity for primary antibodies raised in particular species. Sections were then rinsed in 3 changes of PBS (10 min each) and mounted on glass slides using Vectashield mounting medium (Vector Laboratories, Burlingame, CA).

Sections were examined with a Bio-Rad MRC-1024 confocal laser scanning system equipped with an argon-krypton laser attached to a Nikon Eclipse E800M microscope. Fluorescence of Alexa 488 (green) and Alexa 568 (red) dyes was analyzed using filter configurations for sequential excitation/imaging via 488 nm and 568 nm channels. Digital images were adjusted for brightness and contrast using Photoshop 6.0 software. In each of the confocal immunofluorescence cases some control sections were processed with one of the two primary antibodies omitted. In all cases only the color of the corresponding secondary fluorescent antibody was observed, and only on the appropriate channel. These results indicated that the secondary antibodies were specific for rabbit or mouse IgGs and that there was no “crosstalk” between the red and green channels (Wouterlood et al., 1998).

Electron microscopic double-label immunocytochemistry

For ultrastructural dual localization of TH/CR and TH/PV immunoreactivity, three rats were perfused with the acrolein/paraformaldehyde mixture. To analyze the innervation of PV+ and CR+ interneurons in the BLa by dopaminergic axons, interneurons were selectively stained using antibodies to parvalbumin (PV) or calretinin (CR). Previous studies in our laboratory have shown that both interneuronal subpopulations have high concentrations of their respective calcium-binding proteins, and that both cell bodies and the entire extent of their dendritic arborizations are stained in immunohistochemical preparations (McDonald, 1994; McDonald and Betette, 2001; McDonald and Mascagni, 2001). In some preparations antibodies were diluted in PBS containing 1% normal goat serum and 0.04% Triton X-100, or sections were briefly incubated in PBS containing 1% normal goat serum and 0.04% Triton X-100 for 30 minutes before primary antibody incubation. In other preparations Triton X-100 was omitted because the freeze/thaw technique was used to increase antibody penetration; these sections were cryoprotected in 30% sucrose in PB and freeze-thawed twice over liquid nitrogen. Both preparations were processed using a dual immunoperoxidase method.

Sections were incubated in a cocktail of a mouse monoclonal anti-TH antibody (1:750–1:1000; Chemicon International Inc., Temecula, CA) to identify dopaminergic axon terminals, and in either rabbit anti-PV (1: 1500; Chemicon) or rabbit anti-CR antibodies (1:1500; Chemicon) to identify separate interneuronal subpopulations. All sections were then processed for the avidin-biotin immunoperoxidase technique using a biotinylated goat anti-mouse secondary antibody (1:500; Jackson ImmunoResearch Laboratories, Inc., West Grove, PA) and a Vectastain standard ABC kit (Vector Laboratories, Burlingame, CA). Non-intensified 3,3′-diaminobenzidine (DAB) was used as the chromogen to produce a brown reaction product for TH visualization. After rinsing, sections were incubated in an ABC blocking solution (Avidin/Biotin Blocking kit, Vector Labs), rinsed three times, and then processed for the avidin-biotin immunoperoxidase technique using biotinylated goat anti-rabbit antibodies and a Vectastain Elite ABC kit (Vector Laboratories, Burlingame, CA). CR and PV immunoreactivity was visualized using a Vector VIP (Very Intense Purple) peroxidase substrate kit (Vector Laboratories). This later procedure yielded a reaction product, which we will term “PUR”, that appeared purple in the light microscope, and granular or particulate in the electron microscope (Smiley et al., 1997; Van Haeften and Wouterlood, 2000). For electron microscopy, the penetration of the PUR reaction was similar to that of the DAB reaction, and the particulate

PUR reaction product was easily distinguishable from the diffuse DAB reaction product. The PUR reaction was performed according to the kit's instructions, but the steps in the subsequent dehydration series (see below) were shortened by about 30% to minimize extraction of the purple reaction product (Lanciego et al., 1997).

Sections processed for electron microscopy were postfixed in 1–2% osmium tetroxide in 0.16 M sodium cacodylate buffer (pH 7.4) for 45 minutes, dehydrated in graded ethanols and acetone, and flat embedded in Polybed 812 (Polysciences, Inc., Warrington, PA) in slide molds, between sheets of Aclar (Ted Pella, Inc., Redding, CA). Selected areas of the BLa and BLp were remounted onto resin blanks. Silver thin sections were collected on formvar-coated slot grids, stained with uranyl acetate and lead citrate, and examined with a JEOL-200CX electron microscope. Micrographs were taken with an AMT XR40 digital camera system (Advanced Microscopy Techniques). Figures were then assembled and labeled, and their components' tonal ranges were adjusted and matched in Adobe Photoshop 6.0.

For quantitative analysis, areas were chosen that exhibited robust presence of both labels and that contained at least one labeled interneuronal perikaryon (Fig. 5A) and 4–6 labeled interneuronal dendrites. In all preparations, data analysis focused on the postsynaptic and appositional targets of TH+ axon terminals, and in each case both labeled and unlabeled targets of TH+ terminals were counted. In the TH/PV preparations, two animals were used for quantification. One 60 μm section was chosen per animal. One large area in one section and 4 smaller non-continuous areas in the other section were analyzed. In the TH/CR preparation, two 60 μm sections from one animal and one 60 μm section from a second animal were used for quantification. One large continuous area was selected in the first two preparations, and two smaller non-continuous areas were used in the third preparation. The approximate total area used for quantification was 8000 μm^2 for the TH/CR preparations and 11000 μm^2 for the TH/PV preparations.

Sections from all animals were systematically surveyed. Typically, TH+ axon terminals were followed in 3–7 serial thin sections. Serial sections were helpful for verifying label in small and lightly immunoreactive structures, establishing the synaptic nature of contacts, and identifying multiple targets of individual TH+ terminals. Synaptic contacts were identified based on: 1) parallel spacing of apposed membranes exhibiting membrane thickenings, 2) the presence of dense filaments in the synaptic cleft; and 3) clustered synaptic vesicles associated with the presynaptic membrane (Peters et al., 1991). In the rat amygdala, most synapses formed by TH+ terminals are symmetrical (Asan 1998). Most symmetrical synapses have a narrower synaptic cleft than asymmetric synapses (about 12 nm wide; Peters et al., 1991). Therefore, the widening of synaptic clefts was not considered to be essential for identifying synaptic contacts, as long as the other three criteria for synapses were met. Contacts that did not appear to be synaptic were termed "appositions." Labeled profiles receiving synapses or appositions were identified as perikarya, larger-caliber (>1 μm) and small-caliber (<1 μm) dendrites, and dendritic spines using established morphological criteria (Peters et al., 1991). A Chi-square statistical test was used to compare relative proportions of synaptic contacts onto PV+ versus CR+ structures.

For analysis of TH+ terminals surrounding PV+ somata in basket-like configurations, a total of three areas from TH/PV preparations in the BLp of two animals were chosen at the LM level based on the presence of TH+ baskets. In order to determine synaptic incidence of TH+ terminals forming baskets, 21 TH+ terminals forming basket-like configurations around four cells were followed and completely reconstructed.

Antibody Specificity

The mouse monoclonal TH antibody (Chemicon) was raised against TH purified from PC12 cells and recognizes an epitope on the N-terminus of the protein. Western blot studies conducted by the manufacturer indicate that the antibody recognizes a single line at approximately 59–61 kDa, and does not react with dopamine-beta-hydroxylase, tryptophan hydroxylase, or phenylethanolamine-N-methyltransferase. The rabbit polyclonal TH antibody (Protos Biotech) was raised against bovine TH and stains a single band on Western blots. Preadsorption of the antibody with recombinant TH blocks staining on brain tissue and Western blots in studies performed by the manufacturer. In a previous dual-labeling study of the basolateral amygdala (Asan, 1993) this polyclonal TH antibody was shown to label the same axons as a monoclonal TH antibody obtained from another manufacturer (clone 2/40/15; Boehringer Mannheim Corp.), but did not colabel DBH+ axonal varicosities in the BLC. The mouse monoclonal DBH antibody was raised against purified bovine DBH. It has been used in previous studies to stain noradrenergic cell bodies in the locus ceruleus (Pan et al., 2004) and noradrenergic axons in the brain and spinal cord (Berridge et al., 1996; Stone et al., 1998). Omission of the each of these primary antibodies resulted in a lack of staining.

Because cortical noradrenergic terminals contain much lower levels of TH than dopaminergic terminals, TH immunohistochemistry has been shown to be a relatively selective marker for dopaminergic terminals in the prefrontal cortex (Lewis, 1992; Sesack, 2002). Likewise, previous dual-labeling immunofluorescence studies in the BLC have shown that there are virtually no double-labeled terminals in preparations stained with antibodies to TH and DBH, a selective marker for noradrenergic terminals (Asan, 1993). The only exception was a distinct population of TH+/DBH+ axons with very large varicosities. In the present study we obtained results that are identical to those of Asan (see below). Thus, the TH antibody used in our electron microscopic studies is a fairly selective marker for dopaminergic terminals in the BLC, and was used in a recent study of dopaminergic/cortical interactions in this brain region (Pinto and Sesack, 2008).

RESULTS

Light microscopy

The BLC exhibited a fairly dense innervation by varicose TH-positive (TH+) axons (Fig. 1). Within the BLC the density of TH+ axons in the anterior (BLa) and posterior (BLp) subdivisions of the basolateral nucleus were greater than in the lateral nucleus, but less than that of the central nucleus and intercalated nuclei (Fig. 1A). The axonal varicosities of TH+ fibers were 0.5–1.0 μm in diameter (Fig. 1B). Occasionally axons with distinctly larger varicosities (1.5–2.5 μm) were observed (0–2 per section). Although the examination of Nissl counterstained preparations revealed that the majority of TH+ axons were in the neuropil, some TH+ single varicose axons were found running along the surfaces of Nissl-stained perikarya for 10–15 μm. Pericellular baskets have been described previously in certain nuclei of the BLC (Asan, 1993;Asan, 1997;Brinley-Reed and McDonald, 1999). Our results are consistent with the results of these previous studies; well-differentiated pericellular baskets were more common in the BLp than in the BLa.

In single-labeling immunofluorescence experiments the staining pattern produced by the mouse monoclonal TH antibody was identical to that seen in the immunoperoxidase experiments, and also appeared to be identical to that produced by the rabbit polyclonal TH antibody. In contrast, the density and morphology of axons labeled by the mouse monoclonal DBH antibody was distinctly different. The density of DBH+ fibers in the BLa appeared to be only about one-third to one-half that of the TH+ fibers, and most of the DBH+ axons were straighter, slightly thicker, and had a lower density of varicosities per axonal length than TH

+ axons. A few DBH+ axons with very large varicosities (1.5–2.5 μm) were observed. These axons closely resembled the TH+ axons with large varicosities (see above).

The density of axonal staining produced by each antibody in dual-labeled preparations appeared to be identical to that seen in single-labeled preparations, suggesting that the use of dual-labeling procedures did not interfere with the staining of each individual axonal population. The results of the dual-labeling immunofluorescence experiments indicated that the mouse monoclonal TH antibody used in our preparations primarily stains dopaminergic rather than noradrenergic axons. Thus, the mouse monoclonal TH antibody stained the same axons as the rabbit polyclonal TH antibody used in our previous studies of the dopaminergic innervation of the BLC (Fig 2A; Brinley-Reed and McDonald, 1999). In general, there was no double-labeling of axons in the BLC when the latter antibody was combined with the mouse monoclonal DBH antibody (Fig. 2B). However, occasionally double-labeled TH+/DBH+ axons with distinctive large varicosities (up to 2.5 μm in diameter) were observed (0–2 per section) (Fig. 2C), as anticipated from the single-labeled preparations (see above). The unique morphology and rare occurrence of the latter fibers suggests that they represent the extremely sparse innervation of the basolateral nucleus by TH+/DBH+ axons from the noradrenergic neurons of the caudal lateral brainstem tegmentum (Fallon et al., 1978;Asan, 1993).

Electron microscopy of TH+ terminals and synapses

Electron-dense TH+ terminals were round to ovoid shaped and were characterized by densely-packed, small vesicles that were round and clear (Figs. 3, 5–10). TH+ axon terminals contacted both labeled and unlabeled perikarya, dendrites, and spines in these dual-labeled electron microscopic preparations (Fig. 4; Tables 1–2). Terminals were followed in partial series of thin sections (3–7 sections). In the TH/PV preparation 43.1% (25/58) of TH+ terminals formed synapses (Figs. 3, 6C–D, 8, 9C–D, 10C–D). In the TH/CR preparation 49.2% (31/63) of TH+ terminals formed synapses (Fig. 6A–B). Most terminals forming synapses were 0.4–1.0 μm in diameter, and all synapses were symmetrical. In both TH/PV and TH/CR preparations, the main targets of TH+ terminals were dendrites and spines of unlabeled neurons (Tables 1, 2; Figs. 3, 4).

TH+ innervation of CR+ interneurons

In TH/CR preparations, 16.7% (15/90) of total contacts (including appositions) were onto CR + interneurons (Figs. 4A, 5, 6A–B). CR+ structures constituted 6.4% (2/31) of the total targets of TH+ synapses in TH/CR preparations (Fig. 4A, Table 1). Both of the CR+ postsynaptic targets were small-caliber dendrites (<1 μm diameter; Figs. 4A, 6B). Appositions onto CR+ small-caliber dendrites, large-caliber dendrites (Fig. 6A) and perikarya (Fig. 5C) were also observed (Fig. 4A, Table 1).

TH+ innervation of PV+ interneurons

In TH/PV preparations, 20.5% (17/83) of total contacts including appositions were onto PV+ interneurons (Figs. 4B, 6C–D, 7). PV+ structures constituted 40.0% (10/25) of the total targets of TH+ synapses (Fig. 4B, Table 2). Six of the postsynaptic targets were PV+ small-caliber dendrites (<1 μm diameter; Fig. 6C–D), three were large-caliber dendrites (>1 μm diameter), and one was a PV+ perikaryon (Fig. 4B, Table 2). Appositions onto PV+ small-caliber dendrites (Fig. 7), large-caliber dendrites, and perikarya were also observed (Fig. 4B, Table 2). PV+ dendrites sometimes received several TH+ synaptic contacts when followed in serial sections, and in one case a PV+ dendrite was enveloped by a TH+ axon (Fig. 7). Unlabeled terminals were often found adjacent to TH+ terminals, sometimes forming synapses with the same profile (Fig. 6C–D). Chi-square statistical tests indicated that the percentage of synapses formed by TH+ terminals with PV+ structures (40.0%) was significantly greater than that formed with CR+ structures (6.4%) ($P = 0.007$), and the percentage of TH+ contacts (including appositions)

with PV+ structures that were synapses (58.8% [10/17 contacts]) was significantly greater than the percentage of TH+ contacts with CR+ structures that were synapses (11.8% [2/15 contacts]) ($P = 0.01$).

TH+ axons surrounding PV+ somata in a basket-like configuration have been described in previous light microscopic studies of the rat BLC (Brinley-Reed and McDonald, 1999). These TH+ axonal baskets were also seen in the present material (Figs. 8–10) and were more prominent in the BLp than in the BLa. In order to determine the synaptic incidence of TH+ terminals forming these baskets, complete serial-section reconstructions of TH+ baskets surrounding four PV+ cells in the BLp were conducted. Most of the contacts formed by TH+ terminals involved in basket-like configurations around PV+ perikarya were synapses (76.2% [16/21]; Figs. 8–10). All were symmetrical.

DISCUSSION

The present study is the first investigation to demonstrate that dopaminergic terminals in the rat BLC form synaptic and appositional contacts with both CR+ and PV+ interneuronal subpopulations. Dual labeling immunofluorescence preparations indicate that these TH+ axons mainly represent dopaminergic axons, as shown in previous studies of the amygdala (Asan 1993, 1997). Our quantitative data indicate that PV+ and CR+ cells receive approximately equal percentages of total contacts. However, TH+ contacts onto PV+ structures were much more likely to be synaptic. All synapses formed by TH+ terminals were symmetrical. We have also demonstrated that most of the contacts of TH+ terminals forming basket-like configurations around PV+ perikarya are synapses. As discussed below, the innervation of PV + interneurons by TH+ terminals suggests that dopamine's action on these cells may directly affect inhibitory synaptic transmission, facilitating the induction of long-term potentiation (LTP) and/or oscillatory network activity in the BLC (Bissiere et al., 2003; Loretan et al., 2004).

TH+ innervation of unlabeled neurons

The morphology and distribution of TH+ axons in the BLC seen at the light microscopic level in the present investigation was similar to that described in previous studies (Asan, 1997, 1998; Brinley-Reed and McDonald, 1999). At the ultrastructural level the main targets of TH + terminals were dendrites and spines of unlabeled neurons. This finding is consistent with previous studies in the rat BLC (Asan, 1997) and is also similar to findings in the cerebral cortex (Descarries et al., 1991; Seguela et al., 1988; Verney et al., 1990). Since interneurons constitute only 15% of the total neuronal population in the BLa (McDonald, 1992), most of the unlabeled contacted dendrites, including those that are postsynaptic to TH+ terminals, probably belong to pyramidal cells (McDonald, 1982). In addition, the great majority of spines in the BLa are of pyramidal cell origin (Muller et al., 2006).

In the present study, in which TH+ terminals were partially reconstructed in serial sections, approximately half of all TH+ terminals formed synapses. This is a much greater percentage than that obtained in a single-section analysis of the rat BLC (6.8%; Asan, 1997). However, Asan reported that when a small number of TH+ axon terminals were completely reconstructed in serial sections, virtually all formed synapses (Asan, 1997, 1998). This agrees with observations obtained using extensive serial reconstruction in our laboratory (Muller et al., in press).

TH+ innervation of interneurons in the BLC: Anatomical considerations

The percentage of TH+ contacts with PV+ and CR+ interneurons was less than that with unlabeled presumptive pyramidal cell structures, but higher than expected if there was random

innervation of these interneuronal subpopulations by TH+ terminals. Given that interneurons form about 15% of neurons in the BLa (McDonald, 1992) and PV+ interneurons comprise about 40% of interneurons (McDonald and Mascagni, 2001), PV+ neurons should constitute about 6% of the total neuronal population in the BLa. Likewise, because CR+ neurons comprise about 27% of interneurons in the BLa (Mascagni and McDonald, 2003)[1], CR+ neurons should constitute about 4% of the total neuronal population in this nucleus. In contrast, the percentages of TH+ contacts with PV+ interneurons (20.5%) and CR+ interneurons (16.7%) were 3–4 times higher than the incidence of these interneuronal subpopulations in the BLa. Whereas this suggests that there is a propensity for TH+ axons to contact interneurons, it is important to recall that the areas in the BLa that were selected for analysis were relatively rich in PV+ or CR+ structures.

Similarly, the percentage of TH+ synapses with PV+ interneurons (40%) was also much higher than the incidence of this interneuronal subpopulation in the BLa. Whereas this may also be related in part to the method for selecting areas for analysis, it might also be due to the difficulty in recognizing symmetrical synapses formed by terminals contacting very thin structures such as dendritic spines of unlabeled pyramidal cells. The orientation of these contacts around such small targets is not optimal for recognizing contacts as synapses, especially when full serial section reconstructions are not performed. Thus, we believe that such synapses may have been undercounted in this study. Undercounting synapses with pyramidal cells would inflate the percentage of synapses formed with interneurons. Nevertheless, the fact that synapses with PV + interneurons outnumbered synapses with CR+ interneurons by 6-to-1 (40% versus 6.3%) strongly suggests that PV+ neurons are a preferred target of dopaminergic synapses with interneurons in the BLa.

One of the reasons that appositions were counted in addition to synapses in the present study was that it was sometimes difficult to identify synapses formed by TH+ terminals with certainty. These synapses are usually symmetrical, and often quite small. As a result, synapses that are not oriented perpendicular to the plane of section may not meet the strict morphological criteria for synaptic junctions (see Experimental Procedures). Thus, it is likely that many of the contacts that were classified as “appositions” would actually be classified as synapses if observed in a different orientation, or if complete serial section reconstructions were performed. The other reason for counting appositions was that dopaminergic neurotransmission is not solely dependent on synaptic mechanisms. Dopamine can diffuse into the extracellular space from nonsynaptic terminals, as well as from the region of synaptic junctions, and interact with extrasynaptic receptors (Zoli et al., 1999). In fact, because of the high firing rates and low expression of the plasma membrane dopamine transporter (DAT) in dopaminergic neurons projecting to the BLC (Lammel et al., 2008), the DA uptake rate in the BLC is 10 times less than that exhibited by the striatum (Garris & Wightman, 1994). It has been estimated that DA in the BLC can diffuse about 20 μm before its concentration is reduced by 50%, 8.5 times farther than in the striatum (R. Mark Wightman, University of North Carolina, personal communication). Since dopamine concentrations would be highest in the region immediately surrounding the axon terminal, structures that receive nonsynaptic appositions from TH+ terminals would be prime targets for such dopamine release if they contained dopamine receptors. Unfortunately, there have been no studies of DA receptor expression in distinct subpopulations of interneurons in the BLC.

[1]There is no definitive information regarding the exact percentage of interneurons that are CR+. However, it has been estimated that CR + and VIP+ neurons collectively comprise 30–35% of BLa interneurons, and counts of CR+ neurons in CR+/VIP+ double--labeling material (see Table 3 in Mascagni and McDonald, 2003) suggest that CR+ neurons constitute about 27% of the total interneuronal population.

In TH/CR preparations, 16.7% of total TH contacts (synaptic and appositional combined) were onto CR+ interneurons. However, the percentage of synapses with CR+ structures was low (6.4%) compared with that of PV+ interneurons (40%). Similar to our findings in the BLC, semi-quantitative analyses conducted in monkey cortex by Sesack et al. (1995, 1998) has shown that dopamine axon terminals form synapse-like contacts onto dendrites of PV+ interneurons, but not CR+ interneurons.

In the present study TH+ varicose fibers were often observed surrounding PV+ cell bodies in a basket-like configuration (Figs. 8–10), consistent with a previous light microscopic study performed by our laboratory (Brinley-Reed & McDonald, 1999). Similar TH+ pericellular baskets around GABA-containing neurons are also present in the rat prefrontal cortex, although the synaptic nature of these contacts could not be determined in these light microscopic studies (Benes et al., 1993). Our serial section EM analysis of several of these TH+ baskets in the BLC demonstrated that most of the axons contacting PV+ perikarya formed synapses. In a single-labeled EM study, Asan (1997) found a small number of appositions, but not synapses, with BLC interneuronal somata identified by morphological criteria. However, the interneuronal somata observed by Asan were not surrounded by TH+ axons forming pericellular baskets, and the phenotype of these interneurons could not be determined in that single-labeling study. These differences in the interneurons studied in our investigation versus Asan's may explain the different findings.

TH+ innervation of interneurons in the BLC: Functional implications

The innervation of PV+ interneurons by dopaminergic axons is consistent with several lines of electrophysiological evidence. Although there have been no electrophysiological studies of DA effects on identified PV+ interneurons in the rat BLC, both *in vivo* and *in vitro* investigations have shown that dopamine activates fast-spiking (FS) interneurons in the BLC (Rosenkranz & Grace 1999; Bissiere et al., 2003; Kroner et al., 2005). Since PV+ cells are the main interneurons that are fast-spiking (Rainnie et al., 2006; Woodruff & Sah, 2007b), they are the interneuronal subpopulation most likely influenced by DA (Rosenkranz & Grace 1999; Bissiere et al., 2003; Kroner et al., 2005; 2007).

Dopamine has been shown to enhance feedforward inhibition onto fast-spiking (presumptive PV+) interneurons of the lateral amygdalar nucleus (LA), leading to a reduction in feedforward inhibition onto projection neurons (Bissiere et al., 2003). Dopamine D2 receptors on interneurons are required for this process, and for LTP to occur. Because of extensive synaptic interconnections among PV+ interneurons (Muller et al., 2005; Woodruff and Sah, 2007b), it is possible that the interneurons involved in the DA-induced enhancement of feedforward inhibition onto interneurons are PV+ BLC interneurons.

In addition, dopamine activation of fast-spiking (presumptive PV+) cells induces rhythmic oscillations in the BLC. A study by Loretan et al. (2004) has shown that dopamine increases spontaneous inhibitory network activity and inhibitory oscillations in pyramidal neurons in the LA. In this study, DA application depolarized the majority of fast-spiking interneurons and led to the appearance of synchronized low-frequency oscillations of the inhibitory network (Loretan et al., 2004). PV+ cells have been shown to form interneuronal networks interconnected by GABAergic synapses and gap junctions (Muller et al., 2005; Woodruff & Sah; 2007b). In addition, PV+ cells can make basket-like contacts with as many as 100 perikarya of neighboring pyramidal cells (Rainnie et al., 2006). Thus, the DA-induced increase of BLC pyramidal cell oscillatory activity shown by Loretan et al. (2004) may be mediated by networks of PV+ interneurons that synchronize the outputs of pyramidal cells. (Rainnie et al., 2006; Woodruff & Sah, 2007a,b). Synchronized oscillations of BLC neurons in the theta frequency range are associated with emotional arousal and the consolidation and retrieval of fear memory (Pare and Collins, 2000; Pare et al., 2002; Seidenbecher et al., 2003; Pelletier and

Pare, 2004; Narayanan et al., 2007). The effect of DA on rhythmic oscillations in the BLC has been suggested to decrease spontaneous synaptic input and postsynaptic spikes, increasing the signal to noise ratio, and allowing for the induction of synaptic plasticity (Loretan et al., 2004).

In conclusion, the results of the present investigation suggest that, as in the cortex, dopamine preferentially innervates PV+ versus CR+ interneurons. It is possible that these dopaminergic inputs may differentially innervate certain subpopulations of PV+ cells (Rainnie et al., 2006; Woodruff & Sah; 2007b). Thus, dopamine may synchronize pyramidal cell networks by increasing inhibitory oscillatory activity in one PV+ subpopulation, and may facilitate LTP by suppressing feedforward inhibition via a separate subpopulation.

Acknowledgements

This work was supported by NIH Grant R01-NS38998. We thank Dr. R. Mark Wightman (University of North Carolina) for his calculation of the half-life and diffusion distance of dopamine in the BLa.

Abbreviations

BLa
: anterior subdivision of the basolateral amygdalar nucleus

BLp
: posterior subdivision of the basolateral amygdalar nucleus

BLC
: basolateral nuclear complex of the amygdala

CR
: calretinin

DAB
: 3,3′-diaminobenzidine (DAB)

DBH
: dopamine-beta-hydroxylase

GABA
: gamma aminobutyric acid

LA
: lateral amygdalar nucleus

PB
: phosphate buffer

PBS
: phosphate buffered saline

PUR
: reaction product produced by Vector VIP (Very Intense Purple) substrate kit

PV
: parvalbumin

TH
: tyrosine hydroxylase

Literature Cited

Asan E. Comparative single and double immunolabelling with antisera against catecholamine biosynthetic enzymes: criteria for the identification of dopaminergic, noradrenergic and adrenergic structures in selected rat brain areas. Histochemistry 1993;99(6):427–442. [PubMed: 8104918]

Asan E. Ultrastructural features of tyrosine-hydroxylase-immunoreactive afferents and their targets in the rat amygdala. Cell Tissue Res 1997;288:449–469. [PubMed: 9134859]

Asan E. The catecholaminergic innervation of the rat amygdala. Adv Anat Embryol Cell Biol 1998;142:1–118. [PubMed: 9586282]

Beaudet A, Descarries L. The monoamine innervation of rat cerebral cortex: synaptic and non-synaptic relationships. Neuroscience 1978;3:851–860. [PubMed: 215936]

Ben-Ari Y, Kelly JS. Dopamine evoked inhibition of single cells of the feline putamen and basolateral amygdala. J Physiol London 1976;256:1–21. [PubMed: 933014]

Benes FM, Vincent SL, Molloy R. Dopamine-immunoreactive axon varicosities form nonrandom contacts with GABA-immunoreactive neurons of rat medial prefrontal cortex. Synapse 1993;15:285–95. [PubMed: 8153876]

Benes FM, Berretta S. GABAergic interneurons: implications for understanding schizophrenia and bipolar disorder. Neuropsychopharmacology 2001;25:1–27. [PubMed: 11377916]

Berridge CW, Bolen SJ, Manley MS, Foote SL. Modulation of forebrain electroencephalographic activity in halothane-anesthetized rat via actions of noradrenergic beta-receptors within the medial septal region. J Neurosci 1996;16:7010–7020. [PubMed: 8824337]

Bissière S, Humeau Y, Lüthi A. Dopamine gates LTP induction in lateral amygdala by suppressing feedforward inhibition. Nat Neurosci 2003;6:587–592. [PubMed: 12740581]

Brinley-Reed M, McDonald AJ. Evidence that dopaminergic axons provide a dense innervation of specific neuronal subpopulations in the rat basolateral amygdala. Brain Res 1999;850:127–135. [PubMed: 10629756]

Caine SB, Heinrichs SC, Coffin VL, Koob GF. Effects of the dopamine D-1 antagonist SCH 23390 microinjected into the accumbens, amygdala or striatum on cocaine self-administration in the rat. Brain Res 1995;692:47–56. [PubMed: 8548319]

Carlsen J, Heimer L. The basolateral amygdaloid complex as a cortical-like structure. Brain Res 1988;441:377–380. [PubMed: 2451985]

Cauli B, Audinat E, Lambolez B, Angulo MC, Ropert N, Tsuzuki K, Hestrin S, Rossier J. Molecular and physiological diversity of cortical nonpyramidal cells. J Neurosci 1997;17:3894–3906. [PubMed: 9133407]

Coco ML, Kuhn CM, Ely TD, Kilts CD. Selective activation of mesoamygdaloid dopamine neurons by conditioned stress: attenuation by diazepam. Brain Res 1992;590:39–47. [PubMed: 1422845]

Descarries, L.; Séguéla, P.; Watkins, KC. Nonjunctional relationships of monoamine axon terminals in the cerebral cortex of adult rat. In: Fuxe, K.; Agnati, LF., editors. Volume Transmission in the Brain: Novel Mechanisms for Neural Transmission. Raven Press; New York: 1991. p. 53-62.

Descarries L, Umbriaco D. Ultrastructural basis of monoamine and acetylcholine function in CNS. Semin Neurosci 1995;7:309–318.

Fallon, JH.; Ciofi, P. Distribution of monoamines within the amygdala. In: Aggleton, JP., editor. The Amygdala. Academic Press; New York: 1992. p. 97-114.

Fallon JH, Koziell DA, Moore RY. Catecholamine innervation of the basal forebrain. II. Amygdala, suprarhinal cortex and entorhinal cortex. J Comp Neurol 1978;180:509–532. [PubMed: 659673]

Freund TF, Buzsaki G. Interneurons of the hippocampus. Hippocampus 1996;6:347–470. [PubMed: 8915675]

Garris PA, Wightman RM. Different kinetics govern dopaminergic transmission in the amygdala, prefrontal cortex, and striatum: an in vivo voltammetric study. J Neurosci 1994a;14:442–450. [PubMed: 8283249]

Garris PA, Wightman RM. In vivo voltammetric measurement of evoked extracellular dopamine in the rat basolateral amygdaloid nucleus. J Physiol 1994b;478:239–249. [PubMed: 7965845]

Hancock MB. Two color immunoperoxidase staining: visualization of anatomic relationships between immunoreactive neural elements. Am J Anat 1986;175:343–352. [PubMed: 2422916]

Inglis FM, Moghaddam B. Dopaminergic innervation of the amygdala is highly responsive to stress. J Neurochem 1999;72:1088–1094. [PubMed: 10037480]

Kawaguchi Y. Physiological subgroups of nonpyramidal cells with specific morphological characteristics in layer II/III of rat frontal cortex. J Neurosci 1995;15:2638–2655. [PubMed: 7722619]

Kemppainen S, Pitkänen A. Distribution of parvalbumin, calretinin, and calbindin-D(28k) immunoreactivity in the rat amygdaloid complex and colocalization with gamma-aminobutyric acid. J Comp Neurol 2000;426:441–467. [PubMed: 10992249]

Kilts CD, Anderson CM. Mesoamygdaloid dopamine neurons: differential rates of dopamine turnover in discrete amygdaloid nuclei of the rat brain. Brain Res 1987;416:402–408. [PubMed: 3620969]

Kröner S, Krimer LS, Lewis DA, Barrionuevo G. Dopamine increases inhibition in the monkey dorsolateral prefrontal cortex through cell type-specific modulation of interneurons. Cereb Cortex 2007;17:1020–1032. [PubMed: 16772311]

Kröner S, Rosenkranz JA, Grace AA, Barrionuevo G. Dopamine modulates excitability of basolateral amygdala neurons in vitro. J Neurophysiol 2005;93:1598–1610. [PubMed: 15537813]

Lalumiere RT, Nguyen LT, McGaugh JL. Post-training intrabasolateral amygdala infusions of dopamine modulate consolidation of inhibitory avoidance memory: involvement of noradrenergic and cholinergic systems. Eur J Neurosci 2004;20:2804–2810. [PubMed: 15548223]

Lammel S, Hetzel A, Häckel O, Jones I, Liss B, Roeper J. Unique properties of mesoprefrontal neurons within a dual mesocorticolimbic dopamine system. Neuron 2008;57:760–773. [PubMed: 18341995]

Lanciego JL, Goede PH, Witter MP, Wouterlood FG. Use of peroxidase substrate Vector VIP for multiple staining in light microscopy. J Neurosci Methods 1997;74:1–7. [PubMed: 9210569]

Lewis DA. The catecholaminergic innervation of primate prefrontal cortex. J Neural Transm [Suppl] 1992;36:179–200.

Lewis DA, Pierri JN, Volk DW, Melchitzky DS, Woo TU. Altered GABA neurotransmission and prefrontal cortical dysfunction in schizophrenia. Biol Psychiatry 1999;46:616–626. [PubMed: 10472415]

Lorétan K, Bissière S, Lüthi A. Dopaminergic modulation of spontaneous inhibitory network activity in the lateral amygdala. Neuropharmacology 2004;47:631–639. [PubMed: 15458834]

Mascagni F, McDonald AJ. Immunohistochemical characterization of cholecystokinin containing neurons in the rat basolateral amygdala. Brain Res 2003;976:171–184. [PubMed: 12763251]

McDonald AJ. Neurons of the lateral and basolateral amygdaloid nuclei: a Golgi study in the rat. J Comp Neurol 1982;212:293–312. [PubMed: 6185547]

McDonald, AJ. Cell types and intrinsic connections of the amygdala. In: Aggleton, JP., editor. The amygdala. New York: Wiley-Liss; 1992a. p. 67-96.

McDonald AJ. Projection neurons of the basolateral amygdala: a correlative Golgi and retrograde tract tracing study. Brain Res Bull 1992b;28:179–185. [PubMed: 1375860]

McDonald AJ. Calretinin immunoreactive neurons in the basolateral amygdala of the rat and monkey. Brain Res 1994;667:238–242. [PubMed: 7697361]

McDonald AJ, Betette R. Parvalbumin containing neurons in the rat basolateral amygdala: morphology and colocalization of calbindin D-28k. Neuroscience 2001;102:413–425. [PubMed: 11166127]

McDonald AJ, Mascagni F. Colocalization of calcium-binding proteins and GABA in neurons of the rat basolateral amygdala. Neuroscience 2001;105:681–693. [PubMed: 11516833]

McDonald AJ, Mascagni F. Immunohistochemical characterization of somatostatin containing interneurons in the rat basolateral amygdala. Brain Res 2002;943:237–244. [PubMed: 12101046]

McDonald AJ, Mascagni F. Neuronal localization of 5-HT type receptor immunoreactivity in the rat basolateral amygdala. Neuroscience 2007;146:306–320. [PubMed: 17331657]

McDonald AJ, Muller JF, Mascagni F. GABAergic innervation of alpha type II calcium/calmodulin-dependent protein kinase immunoreactive pyramidal neurons in the rat basolateral amygdala. J Comp Neurol 2002;446:199–218. [PubMed: 11932937]

Muller JF, Mascagni F, McDonald AJ. Synaptic connections of distinct interneuronal subpopulations in the rat basolateral amygdalar nucleus. J Comp Neurol 2003;456:217–236. [PubMed: 12528187]

Muller JF, Mascagni F, McDonald AJ. Coupled networks of parvalbumin immunoreactive interneurons in the rat basolateral amygdala. J Neurosci 2005;25:7366–7376. [PubMed: 16093387]

Muller JF, Mascagni F, McDonald AJ. Pyramidal cells of the rat basolateral amygdala: synaptology and innervation by parvalbumin immunoreactive interneurons. J Comp Neurol 2006;494:635–650. [PubMed: 16374802]

Muller JF, Mascagni F, McDonald AJ. Postsynaptic targets of somatostatin-containing interneurons in the rat basolateral amygdala. J Comp Neurol 2007;500:513–529. [PubMed: 17120289]

Muller JF, Mascagni F, McDonald AJ. Dopaminergic innervation of pyramidal cells in the rat basolateral amygdala. Brain Struct Funct. 2008In Press

Nakano Y, Lénárd L, Oomura Y, Nishino H, Aou S, Yamamoto T. Functional involvement of catecholamines in reward-related neuronal activity of the monkey amygdala. J Neurophysiol 1987;57:72–91. [PubMed: 3559682]

Narayanan RT, Seidenbecher T, Kluge C, Bergado J, Stork O, Pape HC. Dissociated theta phase synchronization in amygdalo- hippocampal circuits during various stages of fear memory. Eur J Neurosci 2007;25:1823–1831. [PubMed: 17408428]

Pan YZ, Li DP, Chen SR, Pan HL. Activation of mu-opioid receptors excites a population of locus coeruleus-spinal neurons through presynaptic disinhibition. Brain Res 2004;997:67–78. [PubMed: 14715151]

Paré D, Collins DR. Neuronal correlates of fear in the lateral amygdala: multiple extracellular recordings in conscious cats. J Neurosci 2000;20:2701–2710. [PubMed: 10729351]

Paré D, Collins DR, Pelletier JG. Amygdala oscillations and the consolidation of emotional memories. Trends Cogn Sci 2002;6:306–314. [PubMed: 12110364]

Paré D, Royer S, Smith Y, Lang EJ. Contextual inhibitory gating of impulse traffic in the intra-amygdaloid network. Ann N Y Acad Sci 2003;985:78–91. [PubMed: 12724150]

Pelletier JG, Paré D. Role of amygdala oscillations in the consolidation of emotional memories. Biol Psychiatry 2004;55:559–562. [PubMed: 15013823]

Peters, A.; Palay, SL.; Webster, HD. The fine structure of the nervous system. New York: Oxford University Press; 1991.

Pezze MA, Feldon J. Mesolimbic dopaminergic pathways in fear conditioning. Mesolimbic dopaminergic pathways in fear conditioning. Prog Neurobiol 2004;74:301–320. [PubMed: 15582224]

Pinto A, Sesack SR. Ultrastructural analysis of prefrontal cortical inputs to the rat amygdala: spatial relationships to presumed dopamine axons and D1 and D2 receptors. Brain Struct Funct 2008;213:159–175. [PubMed: 18340460]

Rainnie DG, Asprodini EK, Shinnick-Gallagher P. Intracellular recordings from morphologically identified neurons of the basolateral amygdala. J Neurophysiol 1993;69:1350–1362. [PubMed: 8492168]

Rainnie DG, Mania I, Mascagni F, McDonald AJ. Physiological and morphological characterization of parvalbumin-containing interneurons of the rat basolateral amygdala. J Comp Neurol 2006;498:142–161. [PubMed: 16856165]

Reynolds GP. Increased concentrations and lateral asymmetry of amygdala dopamine in schizophrenia. Nature 1983;305:527–529. [PubMed: 6621699]

Rosenkranz JA, Grace AA. Modulation of basolateral amygdala neuronal firing and afferent drive by dopamine receptor activation in vivo. J Neurosci 1999;19:11027–11039. [PubMed: 10594083]

Rosenkranz JA, Grace AA. Cellular mechanisms of infralimbic and prelimbic prefrontal cortical inhibition and dopaminergic modulation of basolateral amygdala neurons in vivo. J Neurosci 2002;22:324–337. [PubMed: 11756516]

See RE. Neural substrates of cocaine-cue associations that trigger relapse. Eur J Pharmacol 2005;526:140–146. [PubMed: 16253228]

Séguéla P, Watkins KC, Descarries L. Ultrastructural features of dopamine axon terminals in the anteromedial and the suprarhinal cortex of adult rat. Brain Res 1988;442:11–22. [PubMed: 3359247]

Seidenbecher T, Laxmi TR, Stork O, Pape HC. Amygdalar and hippocampal theta rhythm synchronization during fear memory retrieval. Science 2003;301:846–850. [PubMed: 12907806]

Sesack, SR. Synaptology of dopamine neurons. In: Di Chiara, G., editor. Handbook of Experimental Pharmacology, Dopamine in the CNS I, Vol 154/1. Springer-Verlag; Berlin, Heidelberg: 2002. p. 63-119.

Sesack SR, Hawrylak VA, Melchitzky DS, Lewis DA. Dopamine innervation of a subclass of local circuit neurons in monkey prefrontal cortex: ultrastructural analysis of tryrosine hydroxylase and parvalbumin immunoreactive structures. Cereb Cortex 1998;8:614–622. [PubMed: 9823482]

Smiley JF, Morrell F, Mesulam MM. Cholinergic synapses in human cerebral cortex: an ultrastructural study in serial sections. Exp Neurol 1997;144:361–368. [PubMed: 9168836]

Sorvari H, Soininen H, Pitkänen A. Calretinin-immunoreactive cells and fibers in the human amygdaloid complex. J Comp Neurol 1996;369:188–208. [PubMed: 8726994]

Stone LS, Broberger C, Vulchanova L, Wilcox GL, Hökfelt T, Riedl MS, Elde R. Differential distribution of alpha2A and alpha2C adrenergic receptor immunoreactivity in the rat spinal cord. J Neurosci 1998;18:5928–5937. [PubMed: 9671679]

Van Haeften T, Wouterlood FG. Neuroanatomical tracing at high resolution. J Neurosci Methods 2000;103:107–116. [PubMed: 11074100]

Verney C, Alvarez C, Geffard M, Berger B. Ultrastructural Double-Labelling Study of Dopamine Terminals and GABA-Containing Neurons in Rat Anteromedial Cerebral Cortex. Eur J Neurosci 1990;2:960–972. [PubMed: 12106083]

Washburn MS, Moises HC. Muscarinic responses of rat basolateral amygdaloid neurons recorded in vitro. J Physiol 1992;449:121–154. [PubMed: 1522506]

Wilson JM, Nobrega JN, Corrigall WA, Coen KM, Shannak K, Kish SJ. Amygdala dopamine levels are markedly elevated after self- but not passive-administration of cocaine. Brain Res 1994;668:39–45. [PubMed: 7704616]

Woodruff AR, Sah P. Inhibition and synchronization of basal amygdala principal neuron spiking by parvalbumin-positive interneurons. J Neurophysiol 2007a;98:2956–2961. [PubMed: 17715201]

Woodruff AR, Sah P. Networks of parvalbumin-positive interneurons in the basolateral amygdala. J Neurosci 2007b;27:553–563. [PubMed: 17234587]

Wouterlood FG, Van Denderen JC, Blijleven N, Van Minnen J, Härtig W. Two-laser dual-immunofluorescence confocal laser scanning microscopy using Cy2- and Cy5-conjugated secondary antibodies: unequivocal detection of co-localization of neuronal markers. Brain Res Brain Res Protoc 1998;2:149–159. [PubMed: 9473644]

Yang CR, Seamans JK, Gorelova N. Developing a neuronal model for the pathophysiology of schizophrenia based on the nature of electrophysiological actions of dopamine in the prefrontal cortex. Neuropsychopharmacology 1999;21:161–194. [PubMed: 10432466]

Zoli M, Jansson A, Syková E, Agnati LF, Fuxe K. Volume transmission in the CNS and its relevance for neuropsychopharmacology. Trends Pharmacol Sci 1999;20:142–150. [PubMed: 10322499]

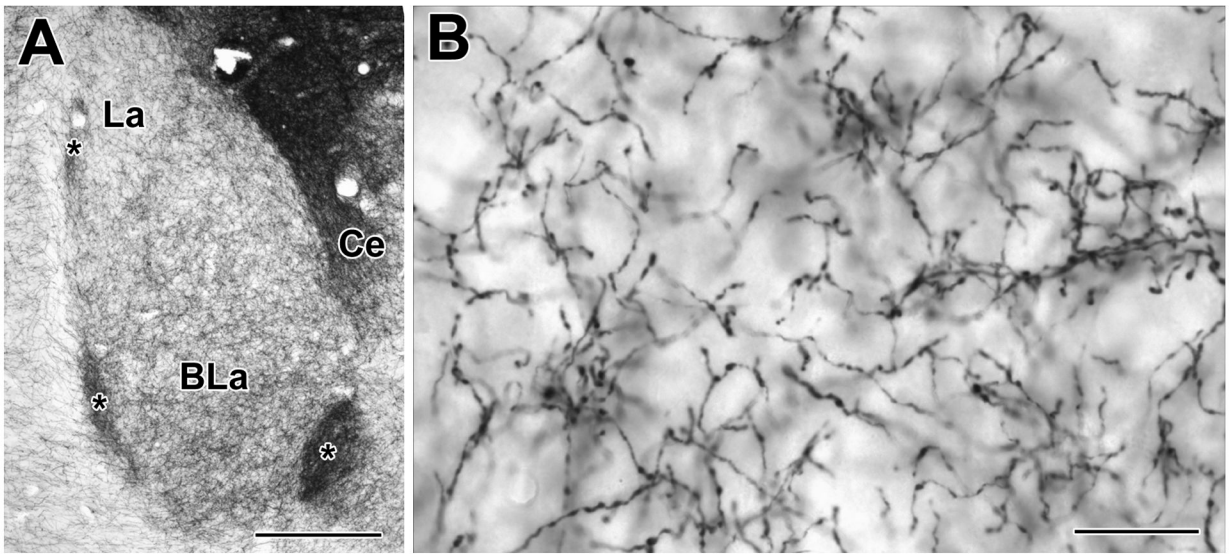

Fig. 1.

Digital photomicrographs of tyrosine hydroxylase (TH) immunoreactivity in the rat basolateral amygdala, using Ni-DAB as a chromogen. A) Low-power micrograph illustrating TH immunoreactivity in the anterior basolateral (BLa) and lateral (La) nuclei (Bregma −2.56 level of Paxinos and Watson, 1997; medial is to the right). Ce = central amygdalar nucleus; asterisks indicate intercalated nuclei. B) Higher power micrograph illustrating the morphology of TH+ axons in the BLa. Scale bars = 200 μm in A and 20 μm in B.

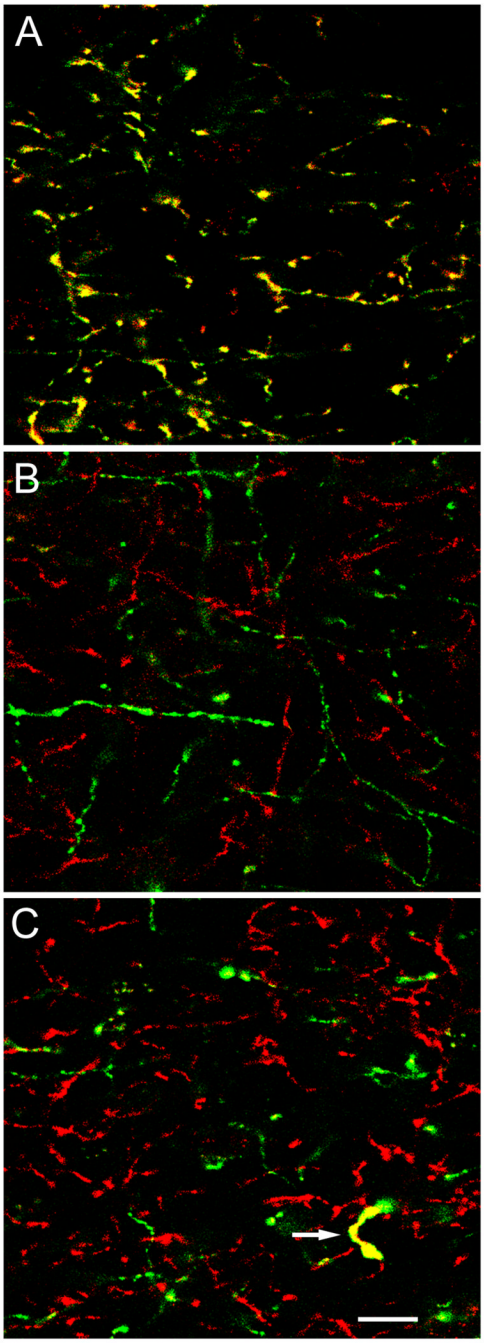

Fig. 2.

Confocal microscopy of TH and DBH immunoreactivity in the BLC. Red and green channels are merged in all three images. Double-labeled structures appear yellow. A) Dual labeling of axons in the BLa by the mouse monoclonal TH antibody (green) and the rabbit polyclonal TH antibody (red). Virtually all axons are double-labeled (yellow). B) Dual localization of DBH (green; monoclonal DBH antibody) and TH (red; rabbit polyclonal TH antibody) in the BLa. No axons are double-labeled. C) Dual localization of DBH (green; monoclonal DBH antibody) and TH (red; rabbit polyclonal TH antibody) in the BLa. The only TH+ axon in this field that was also DBH+ (arrow) had a very distinctive morphology. It had large varicosities, and the

intervaricose portions were thicker than that of most other TH+ axons. Scale bar = 10 μm for all three images.

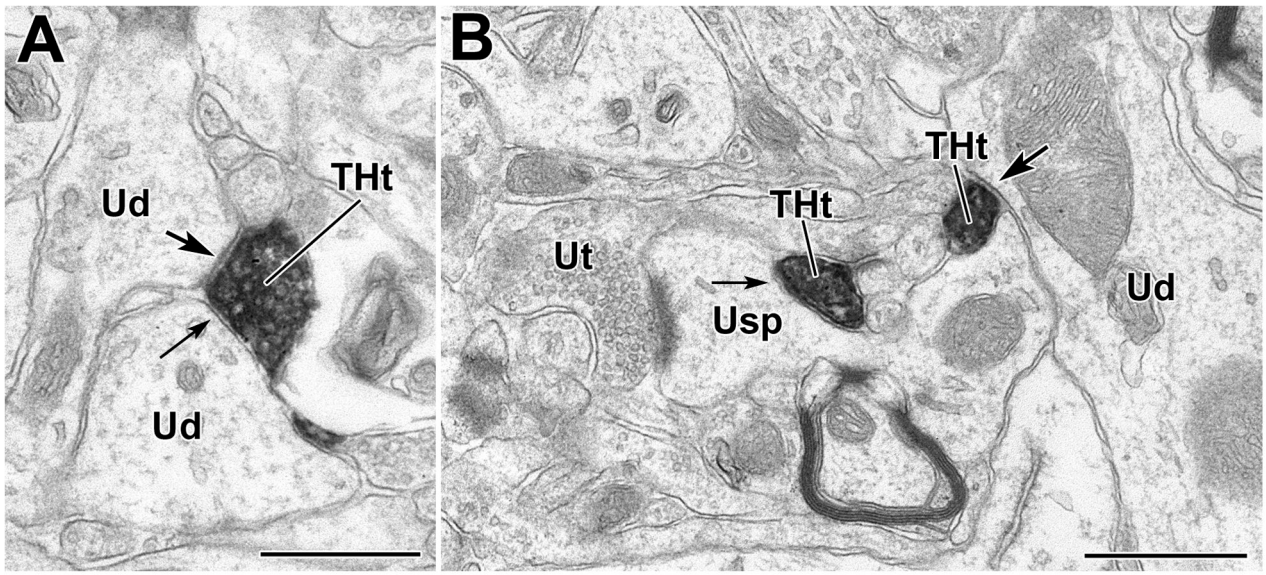

Fig. 3.

TH+ terminals innervate unlabeled dendrites and spines in the BLa. A) A DAB-labeled TH+ terminal (THt) forms a synapse (arrow with large arrowhead) and an apposition (arrow with small arrowhead) with thin unlabeled dendrites (Ud). B) A DAB-labeled TH+ terminal makes an apposition (arrow with small arrowhead) with an unlabeled spine neck. The head of this spine also receives an asymmetric synapse from an unlabeled axon terminal (Ut). Also in this field is an unlabeled dendrite (Ud) receiving synaptic input (arrow with large arrowhead) from a separate TH+ terminal (THt). Both micrographs are from TH/PV preparations, but there are no PUR labeled PV+ structures in this field. Scale bars = 500 nm.

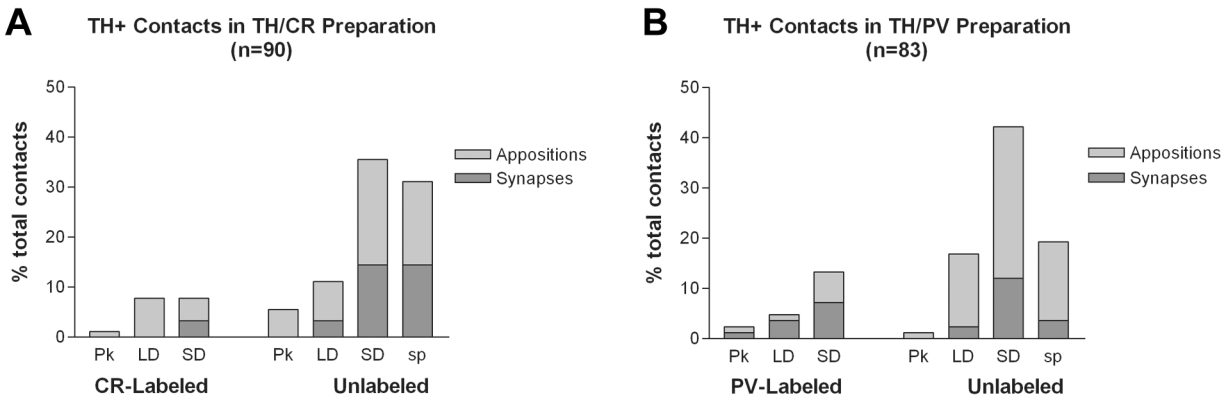

Fig. 4.

Histogram showing the percentage of synaptic (dark gray) and appositional (light gray) targets of TH+ terminals partially reconstructed from serial sections (3–7 serial sections each) from BLa areas dual-labeled for TH/CR (A) or TH/PV (B). Abbreviations: Pk = perikarya, LD = large dendrites (>1μm thick), SD = small dendrites (<1μm thick), sp = spines.

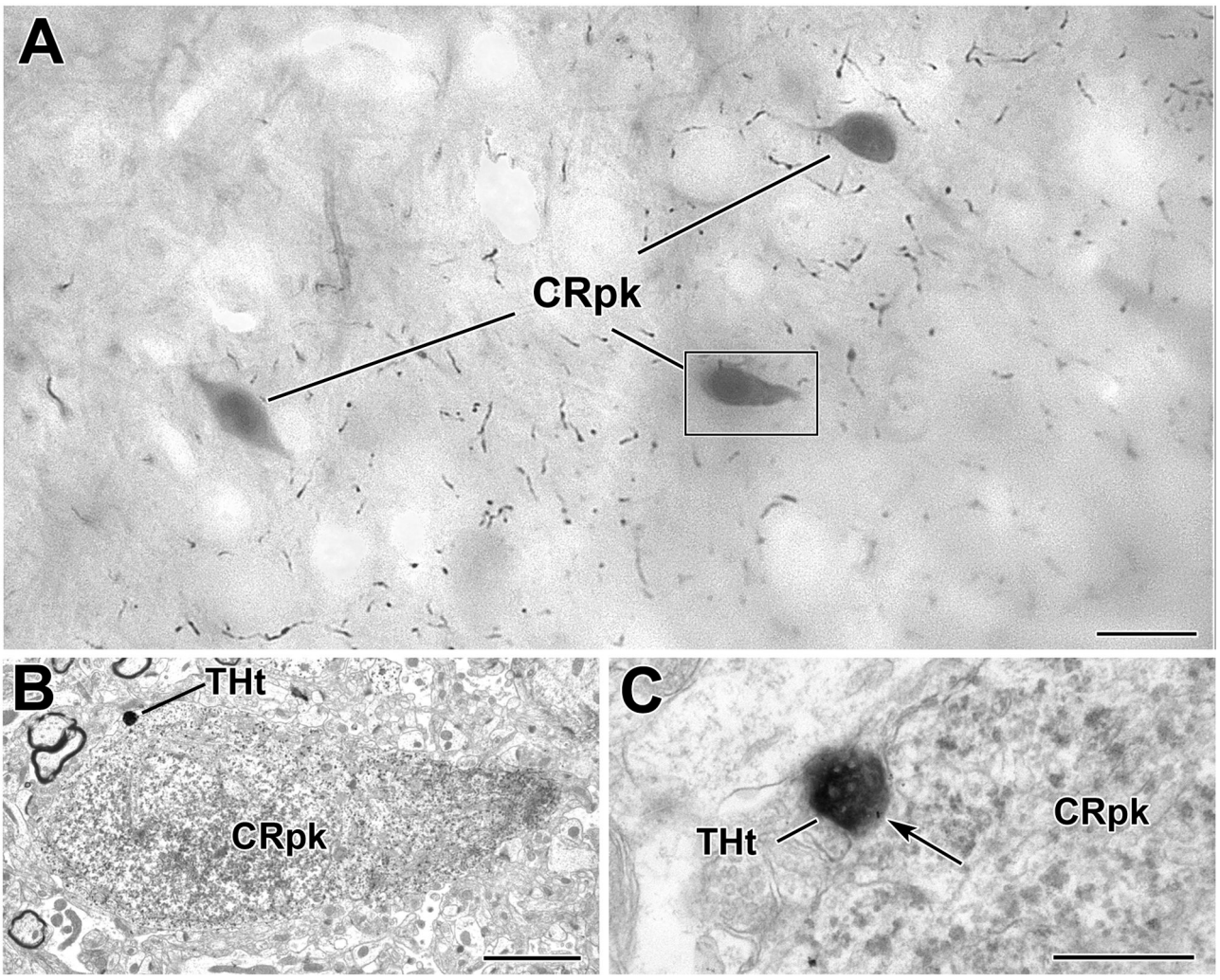

Fig. 5.

A TH+ terminal contacts a CR+ perikaryon in the BLa. A) Low power photomicrograph (grayscale image) of an osmicated, resin−embedded section showing three PUR-immunostained CR+ perikarya (CRpk) in the BLa at the bregma −2.8 level. Most of the varicose axons in the neuropil are TH+. The perikaryon in the box is shown in B. B) Electron micrograph of a CR-immunoreactive perikaryon. The TH+ terminal (THt) contacting the CR + perikaryon is shown in C. C) Higher power electron micrograph of the DAB-labeled TH+ terminal forming an apposition (arrow) with the PUR-labeled CR+ perikaryon shown in B. Note the particulate PUR reaction product in the CR+ perikarya. Scale bars = 10 μm in A, 2 μm in B and 500 nm in C.

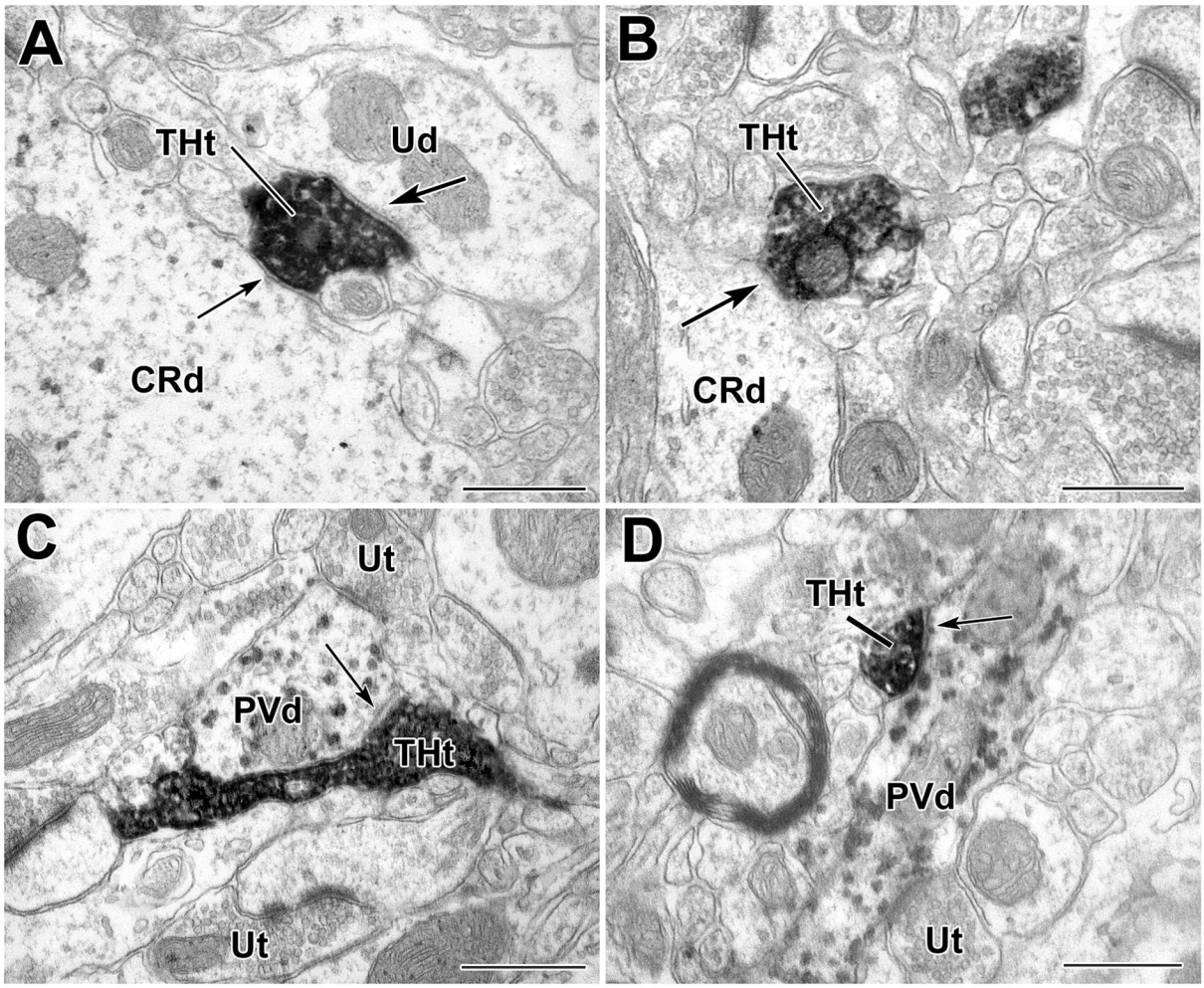

Fig. 6.

TH+ terminals contact CR+ and PV+ dendrites in the BLa. A) A DAB-labeled TH+ terminal (THt) forms a synaptic contact (arrow with large arrowhead) with a small unlabeled dendrite (Ud) and an apposition (arrow with small arrowhead) with a large PUR-labeled CR+ dendrite (CRd). B) A small PUR-labeled CR+ dendrite (CRd) receives synaptic input (arrow) from a DAB-labeled TH+ terminal. C–D) PUR-labeled PV+ dendrites (PVd) receive synaptic input (arrows) from DAB-labeled TH+ terminals (THt). Scale bars = 500 nm.

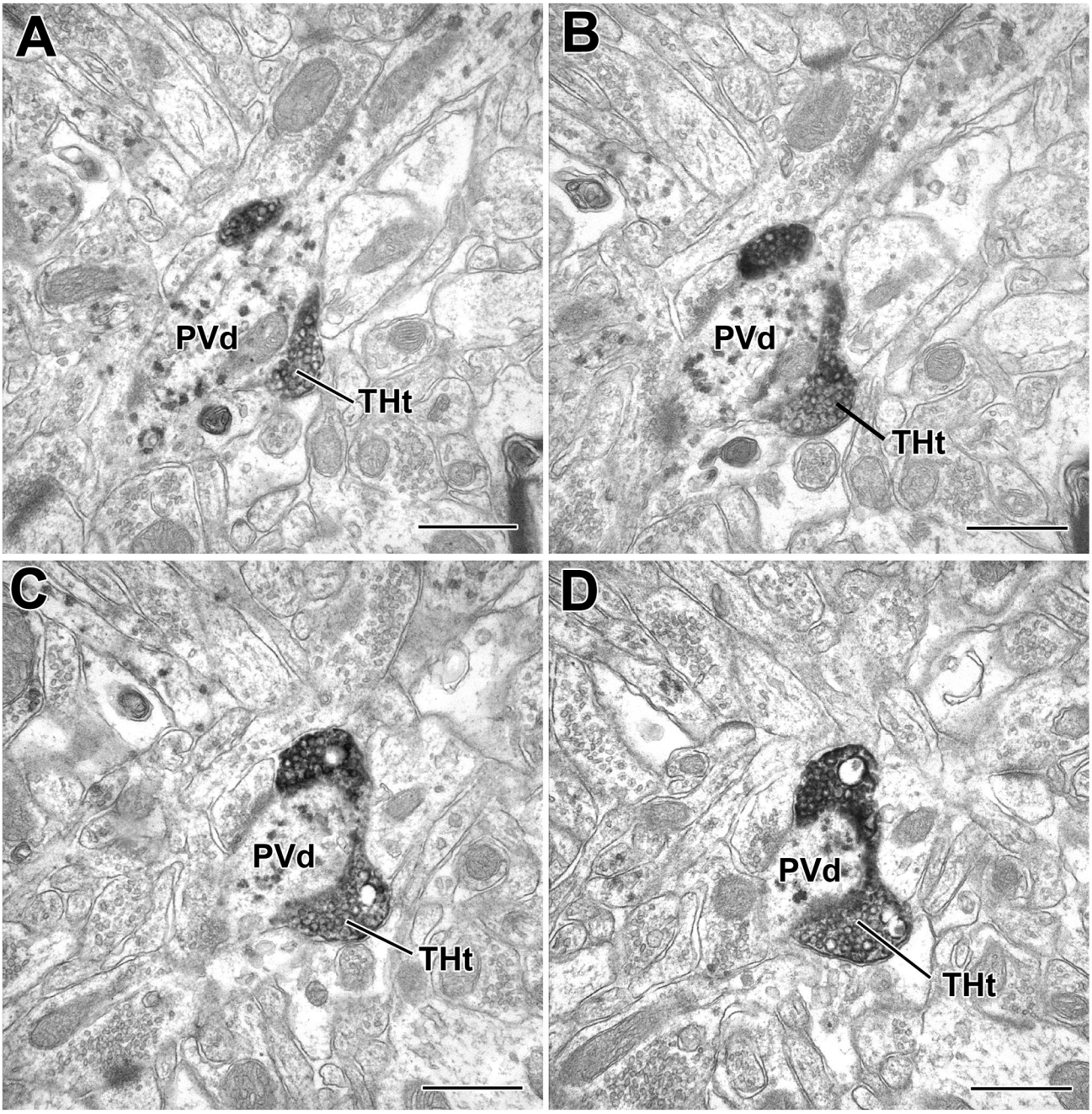

Fig. 7.

A PV+ dendrite enveloped by a TH+ axon in the BLa. Serial sections (A–D) of a DAB-labeled TH+ axon (THt) that forms an extended apposition with a PUR-labeled PV+ small dendrite (PVd). Although portions of the apposition resembled an obliquely cut synapse, at no point were all of the criteria for a synaptic junction met. Scale bars = 500 nm.

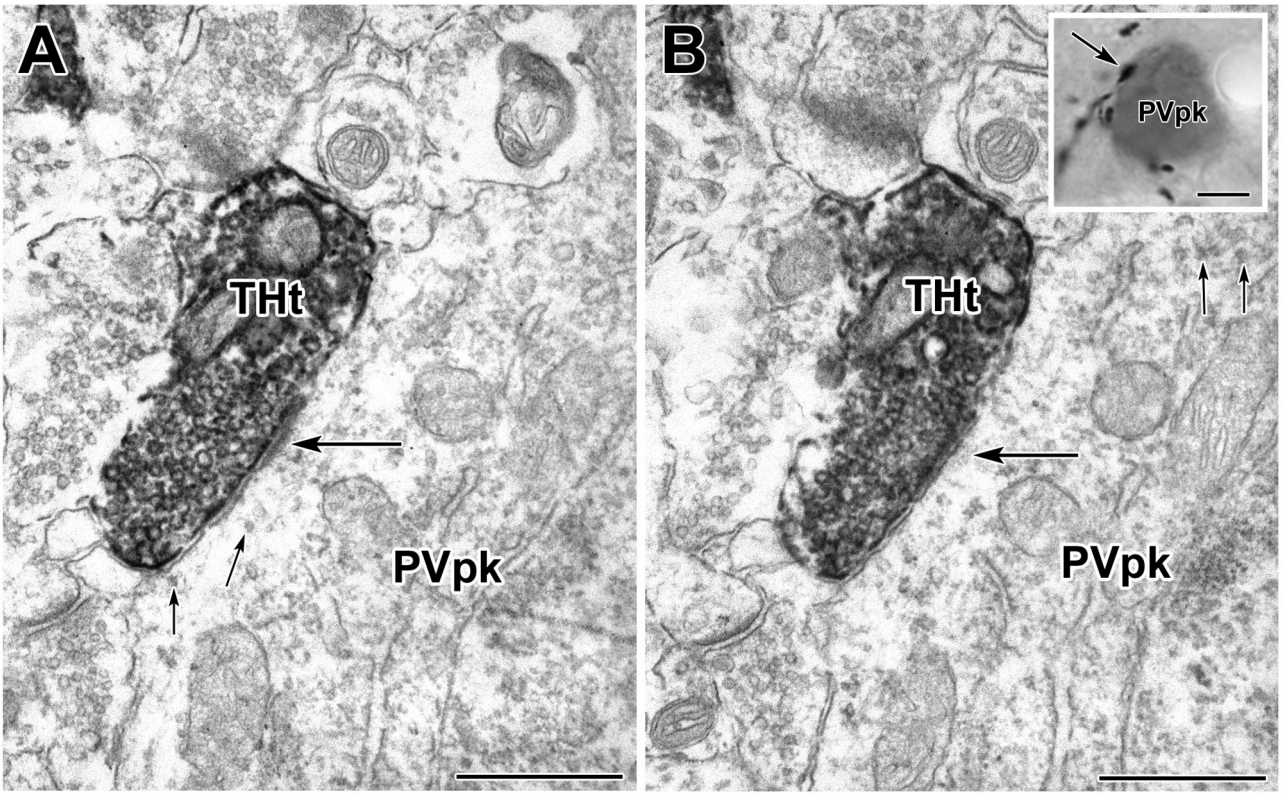

Fig. 8.

A PV+ perikaryon is enveloped by TH+ axons in a basket-like configuration (see inset in B). A–B) Two serial sections through the PUR-labeled PV+ perikaryon (PVpk) receiving a synaptic contact (large arrows) from the DAB-labeled TH+ terminal (THt) shown in the inset in B (arrow). Smaller arrows indicate the PUR label. Scale bars = 500 nm in A and B, 4 μm in inset in B.

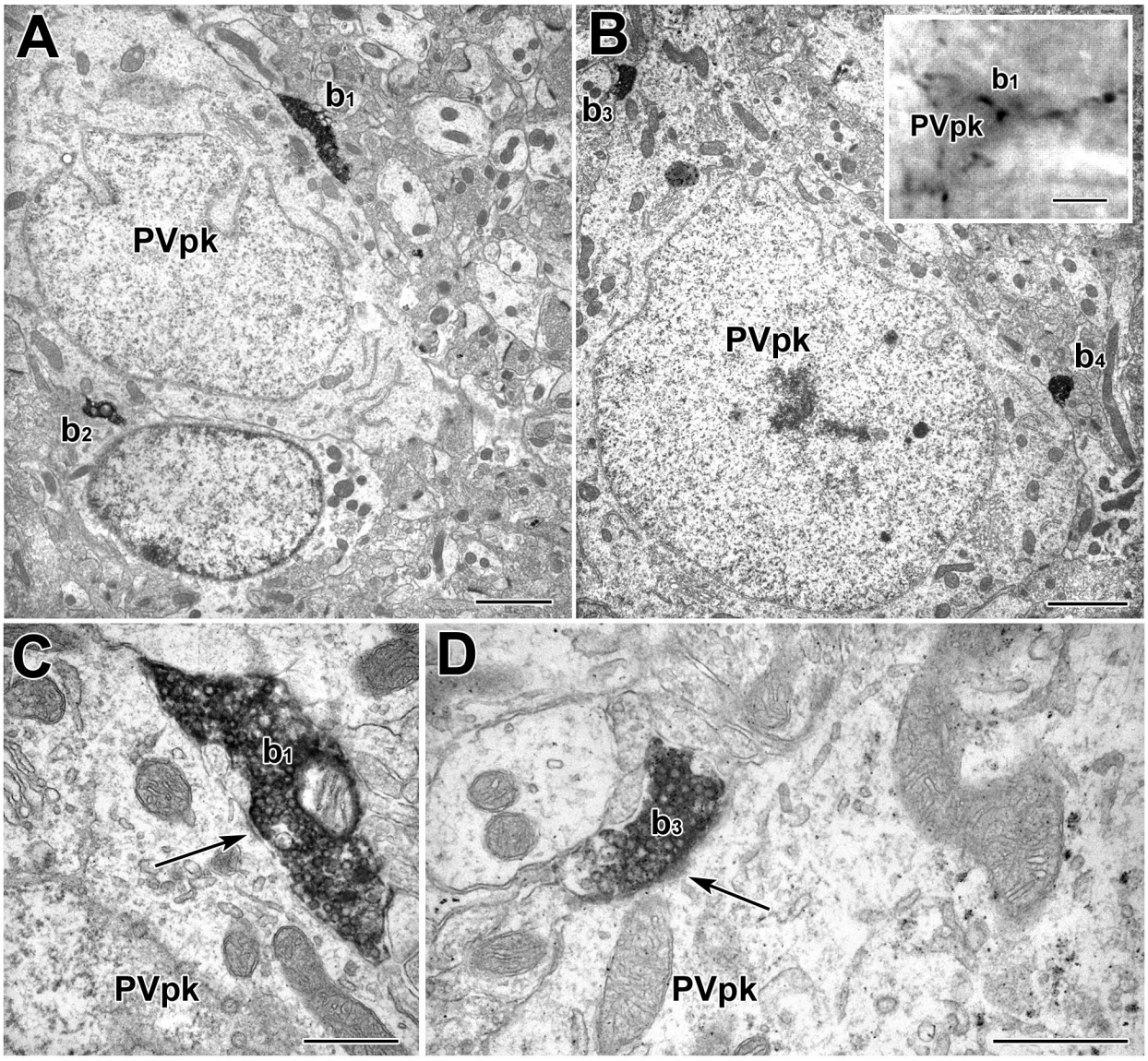

Fig. 9.

A PV+ perikaryon (PVpk) is enveloped by TH+ axons in a basket-like configuration (see inset in B). A–B) Two sections through the PUR-labeled PV+ perikaryon receiving synaptic contacts (arrows) from DAB-labeled TH+ terminals (b1–b4). C) Higher power view of the contact formed by TH+ terminal b1. Arrow indicates part of the synaptic junction. D: Higher power view of the contact formed by TH+ terminal b3. Arrow indicates part of the synaptic junction. Scale bars = 2 μm in A and B, 5 μm in inset in B, 500 nm in C and D.

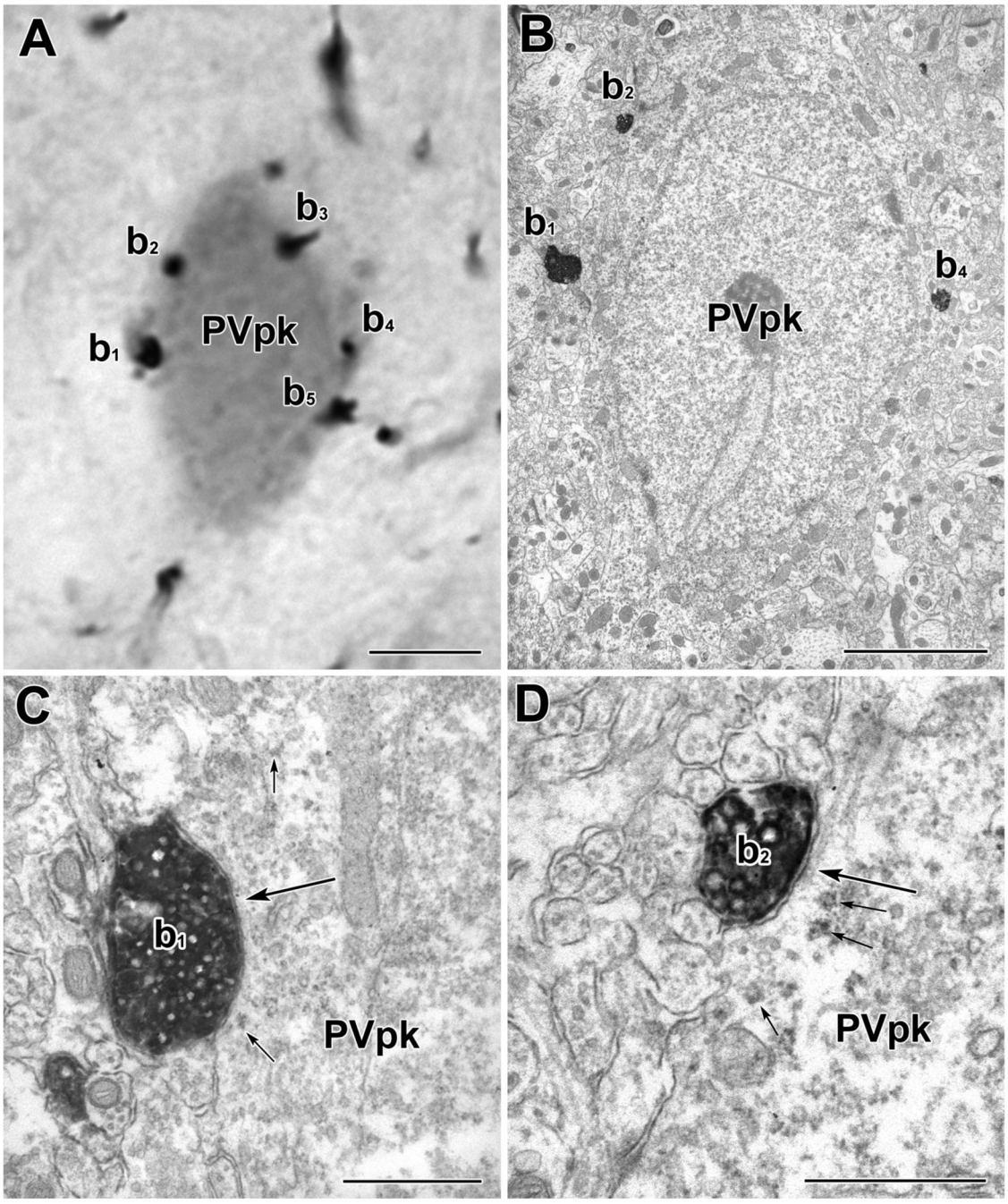

Fig. 10.

A PV+ perikaryon is enveloped by TH+ axons in a basket-like configuration. A) Light micrograph of a PUR-labeled PV+ perikaryon (PVpk) receiving apparent contacts from DAB-labeled TH+ terminals (b1–b5). B) Electron micrograph of the PUR-labeled PV+ perikaryon (PVpk) shown in A. C) Higher power view of the contact (large arrow) formed by TH+ terminal b1. This contact was considered to be a synapse with a narrow synaptic cleft (see Experimental Procedures). Small arrows indicate examples of PUR label. D) Higher power view of the contact (large arrow) formed by TH+ terminal b2. This contact was considered to be a small synapse. There is a pronounced density in the synaptic cleft. A cluster of synaptic vesicles

adjacent to the presynaptic membrane was more obvious in an adjacent thin section. Small arrows indicate examples of PUR label. Scale bars = 5 μm in A and B, 500 nm in C and D.

TABLE 1

Targets of tyrosine hydroxylase-positive terminals (n = 63) in the anterior subdivision of the basolateral nucleus in preparations dual-labeled for TH and CR.

Postsynaptic targets	CR+ Pk	CR+ LD	CR+ SD	Unlabeled Pk	Unlabeled LD	Unlabeled SD	Unlabeled spines	Total
Number (%) of TH contacts:	1 (1.1)	7 (7.8)	7 (7.8)	5 (5.6)	10 (11.1)	32 (35.5)	28 (31.1)	90 (100)
Number (%) of TH synapses:	0 (0)	0 (0)	2 (6.4)	0 (0)	3 (9.6)	13 (42.0)	13 (42.0)	31 (100)

Abbreviations: Pk=perikarya; LD=large dendrite (>1μm); SD=small dendrite (<1μm);

TABLE 2

Targets of tyrosine hydroxylase-positive terminals (n = 58) in the anterior subdivision of the basolateral nucleus in preparations dual-labeled for TH and PV.

Postsynaptic targets	PV+ Pk	PV+ LD	PV+ SD	Unlabeled Pk	Unlabeled LD	Unlabeled SD	Unlabeled spines	Total
Number (%) of TH contacts:	2 (2.4)	4 (4.8)	11 (13.2)	1 (1.2)	14 (16.9)	35 (42.2)	16 (19.3)	83 (100)
Number (%) of TH synapses:	1 (4.0)	3 (12.0)	6 (24.0)	0 (0)	2 (8.0)	10 (40.0)	3 (12.0)	25 (100)

Abbreviations: Pk=perikarya; LD=large dendrite (>1μm); SD=small dendrite (<1μm).